Geophysical Research Letters

RESEARCH LETTER
10.1029/2024GL110525

Implications of a Pervasive Climate Model Bias for Low-Cloud Feedback

P. Ceppi[1], T. A. Myers[2,3], P. Nowack[4,5], C. J. Wall[6], and M. D. Zelinka[7]

[1]Department of Physics, Imperial College London, London, UK, [2]Cooperative Institute for Research in Environmental Sciences, University of Colorado Boulder, Boulder, CO, USA, [3]Physical Science Laboratory, National Oceanic and Atmospheric Administration, Boulder, CO, USA, [4]Institute of Theoretical Informatics, Karlsruhe Institute of Technology, Karlsruhe, Germany, [5]Institute of Meteorology and Climate Research (IMK-ASF), Karlsruhe Institute of Technology, Karlsruhe, Germany, [6]Department of Geosciences, University of Oslo, Oslo, Norway, [7]Lawrence Livermore National Laboratory, Livermore, CA, USA

Abstract How low clouds respond to warming constitutes a key uncertainty for climate projections. Here we observationally constrain low-cloud feedback through a controlling factor analysis based on ridge regression. We find a moderately positive global low-cloud feedback (0.45 W m^{-2} K^{-1}, 90% range 0.18–0.72 W m^{-2} K^{-1}), about twice the mean value (0.22 W m^{-2} K^{-1}) of 16 models from the Coupled Model Intercomparison Project. We link this discrepancy to a pervasive model mean-state bias: models underestimate the low-cloud response to warming because (a) they systematically underestimate present-day tropical marine low-cloud amount, and (b) the low-cloud sensitivity to warming is proportional to this present-day low-cloud amount. Our results hence highlight the importance of reducing model biases in both the mean state of clouds and their sensitivity to environmental factors for accurate climate change projections.

Plain Language Summary Low clouds have a large impact on climate by reflecting a portion of incoming sunlight back to space. Hence any future changes in clouds under global warming could amplify or dampen climate change—a phenomenon known as "cloud feedback." Climate models however disagree on future low-cloud changes, resulting in large uncertainty in future global-warming projections. Here we perform a statistical analysis of global satellite observations of low clouds, using observed co-variations between clouds and meteorology to constrain the feedback simulated by climate models. We find evidence of an amplifying feedback by low clouds, stronger than simulated by most climate models. We link this discrepancy to a low-cloud deficit across wide swathes of the tropical oceans characterized by abundant low cloud cover in observations. Thus to reduce climate projection uncertainty, we propose it is important to understand and mitigate the low-cloud deficit in climate models.

Key Points:

- We implement a statistical learning-based analysis to constrain low-cloud feedback, with strong out-of-sample predictive skill
- The observationally constrained global-mean feedback is about double the mean value from an ensemble of 16 climate models
- This discrepancy is consistent with a pervasive underestimate of mean-state tropical marine low-cloud amount in the models

Supporting Information:

Supporting Information may be found in the online version of this article.

Correspondence to:

P. Ceppi,
p.ceppi@imperial.ac.uk

Citation:

Ceppi, P., Myers, T. A., Nowack, P., Wall, C. J., & Zelinka, M. D. (2024). Implications of a pervasive climate model bias for low-cloud feedback. *Geophysical Research Letters*, *51*, e2024GL110525. https://doi.org/10.1029/2024GL110525

Received 29 JAN 2024
Accepted 30 SEP 2024

© 2024. The Author(s).
This is an open access article under the terms of the Creative Commons Attribution License, which permits use, distribution and reproduction in any medium, provided the original work is properly cited.

1. Introduction

Clouds have long been known as a key driver of uncertainty in climate sensitivity, particularly through the feedback of marine low clouds (Bony & Dufresne, 2005; Boucher et al., 2013; Charney et al., 1979; Sherwood et al., 2020; Zelinka et al., 2020). Given the known limitations of climate models in simulating cloud processes, it is of interest to instead turn to global satellite observations to constrain this low-cloud feedback.

One commonly used observational approach involves approximating cloud-radiative anomalies in terms of their responses to a set of physically based meteorological "cloud-controlling factors" (Stevens & Brenguier, 2009). If the relationships between clouds and their controlling factors can be estimated sufficiently accurately from observations, they can then be used to constrain the cloud responses to the expected future controlling factor changes under global warming, that is, the cloud feedback. Numerous studies have applied this approach to marine tropical low clouds, generally finding evidence of a positive low-cloud feedback in a manner consistent with moderate climate sensitivity values (e.g., Brient & Schneider, 2016; Cesana & Del Genio, 2021; Myers & Norris, 2016; Myers et al., 2021; Qu et al., 2015).

A recent advance in cloud-controlling factor analysis has been the implementation of regression regularization methods, particularly ridge regression (Andersen et al., 2023; Ceppi & Nowack, 2021; Wilson Kemsley et al., 2024). Compared with traditional non-regularized multiple least squares regression, ridge regression allows us to include a greater number of predictors, thus leading to improved out-of-sample prediction skill, especially in

contexts with many collinear predictors (Dormann et al., 2013; Nowack et al., 2023). For example, Ceppi and Nowack (2021) included controlling factors from surrounding grid points, instead of strictly local predictors as in previous studies. A limitation of their study, however, is that their data did not discriminate between contributions from different cloud regimes—for example, low versus free-tropospheric clouds. This motivates a new observational controlling factor analysis of low-cloud feedback, using regularized regression with non-local predictors.

Previous studies have linked low-cloud feedback to various biases in the mean-state cloud climatology: for example, involving biases in low-cloud radiative effects (Brient & Bony, 2012), the occurrence of specific cloud regimes (Cesana et al., 2023; Kuma et al., 2023), or the meridional distribution of cloud albedo (Siler et al., 2018). Here we focus on the known severe underrepresentation of low-cloud amount in global climate models (Cesana et al., 2023): particularly in regions of strong subsidence, the average climate model from the Coupled Model Intercomparison Project phases 5 and 6 (CMIP5/6) underestimates low-cloud amount by a factor of around two (Figure 1). Note that this low-cloud amount deficit cannot be ascribed to sea-surface temperature (SST) biases, since similar results are obtained from AMIP simulations forced with observed SSTs (Figure S1 in Supporting Information S1), and furthermore it is not accounted for by differences in obscuration by high clouds (not shown).

Models compensate for their low-cloud amount deficit by simulating unrealistically reflective clouds—the "too few, too bright" problem, persisting across generations of global climate models (Črnivec et al., 2023; Klein et al., 2013; Konsta et al., 2022; Nam et al., 2012; Zhang et al., 2005). Here we provide novel evidence that this pervasive low-cloud amount deficit in models has implications for their simulation of low-cloud feedback.

2. Data and Methods

2.1. Observational, Reanalysis, and Climate Model Data

We analyse data from five global satellite data sets of cloud properties: the Moderate Resolution Imaging Spectroradiometer (MODIS) combined Aqua/Terra cloud property data set, collection 6.2 (Pincus et al., 2023); the Clouds and the Earth's Radiant Energy System (CERES) Flux-By-Cloud-Type (FBCT) data set Edition 4.1 (Sun et al., 2022); the International Satellite Cloud Climatology Project (ISCCP) H-series (Young et al., 2018); the Pathfinder Atmospheres Extended data record (PATMOS-x; Heidinger et al., 2014); and the Cloud_cci Advanced Very High Resolution Radiometer post meridiem (AVHRR-PM) data set version 3 (Stengel et al., 2020). For each data set we use a minimum of 20 years of monthly data. Table S1 in Supporting Information S1 summarizes the analysis periods for each data set.

All of the above satellite data sets provide global gridded observations of cloud amount binned by cloud top pressure (CTP) and cloud optical depth (τ), often described as "cloud amount histograms," from which radiative anomalies associated with low clouds can be inferred, as described in Section 2.2 below.

To relate the cloud property variations to meteorological cloud-controlling factors, we use data from the fifth generation of the European Center for Medium-Range Weather Forecasts (ECMWF) atmospheric reanalysis of the global climate (ERA5; Hersbach et al., 2020). Six cloud-controlling factors (described in Section 2.3 below) are calculated from four surface and near-surface variables (sea-level pressure, surface skin temperature, zonal and meridional components of the 10-m wind), as well as three variables at 700 hPa (air temperature, relative humidity, vertical pressure velocity), all of which are in monthly mean resolution.

We additionally analyse similar output from global climate model simulations available from the Coupled Model Intercomparison Project phases 5 and 6 (CMIP5, CMIP6; Eyring et al., 2016; Taylor et al., 2012). We use the historical experiment for the 20-year period January 1981–December 2000; the experiment and period are chosen to be as comparable as possible to the observations, noting that the CMIP5 historical simulations end in 2005. Cloud amount histograms are obtained from the ISCCP satellite simulator output (Bodas-Salcedo et al., 2011), which facilitates comparison with satellite observations. Furthermore, we use the same seven meteorological variables as obtained from the ERA5 reanalysis to calculate cloud-controlling factors. Table S2 in Supporting Information S1 lists the 16 CMIP5 and CMIP6 models that provide the necessary satellite simulator data.

Prior to analysis, we regrid all data to a common $5° \times 5°$ longitude–latitude grid, using conservative remapping for cloud amount, and bilinear remapping for the meteorological variables.

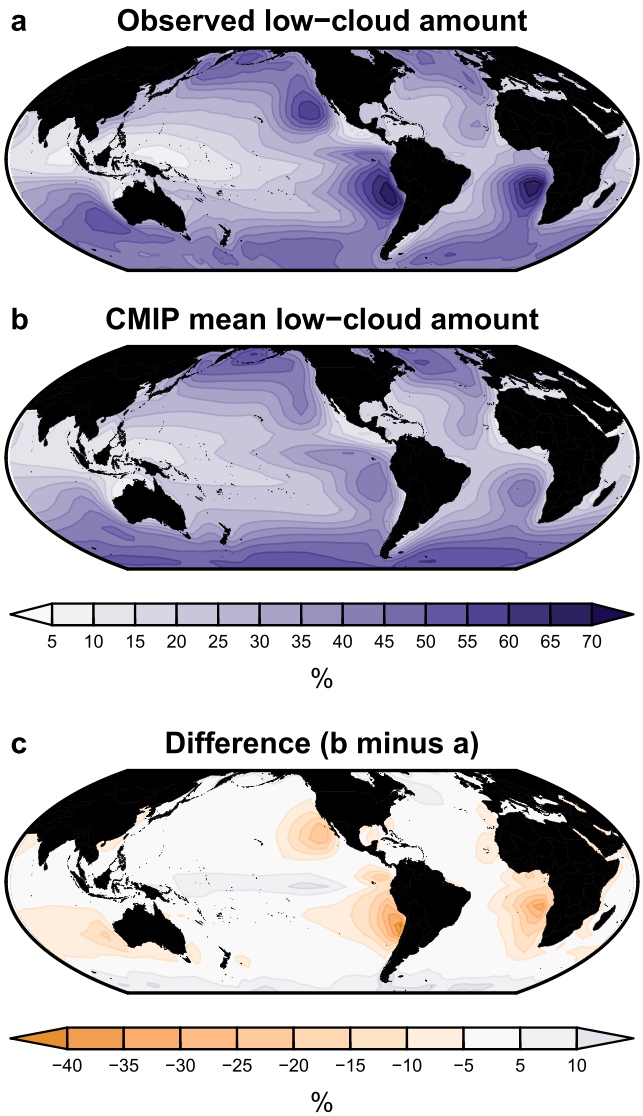

Figure 1. Maps of climatological marine low-cloud amount for (a) the mean of five observational data sets (Table S1 in Supporting Information S1) during their common period July 2002–June 2009, (b) the CMIP multi-model mean historical climate during 1981–2000, and (c) their difference. CMIP low-cloud amount is taken from ISCCP satellite simulator data to ensure a fair comparison with satellite observations. For both CMIP models and observations, we exclude the lowest optical depth bin prior to integrating over all low-cloud histogram bins, to exclude known artifacts and biases in observational products (Pincus et al., 2012).

2.2. Cloud-Radiative Anomalies

For MODIS, CERES and AVHRR-PM observations, we define low clouds as having CTP >680 hPa, corresponding to the two cloud histogram pressure levels closest to the surface. ISCCP and PATMOS-x have documented biases in their CTP retrievals, such that a substantial amount of low cloud scenes are erroneously attributed to the third highest pressure level 560< CTP <680 hPa (Garay et al., 2008; Myers et al., 2021; Qu et al., 2015), and we show that this bias is reproduced in CMIP ISCCP simulator output (Text S1 and Figure S2 in Supporting Information S1). Therefore for these data sets, we use CTP >560 hPa as our low-cloud definition. In all cases, low-cloud amount anomalies are adjusted for high-cloud overlap (Text S2 in Supporting Information S1).

To obtain the radiative anomalies associated with low-cloud variations, we apply the cloud-radiative kernels developed by Zelinka et al. (2012) to monthly deseasonalized cloud histogram anomalies, and follow the method of Scott et al. (2020) and Myers et al. (2021). Further details are provided in Text S2 in Supporting Information S1.

2.3. Cloud-Controlling Factor Analysis

Cloud-controlling factor analysis relates cloud property variations to anomalies in meteorological *controlling factors*, taken to be proxies for processes regulating the physical properties of clouds. The approach has been widely applied to interpret the variability of marine low clouds and their response to global warming (e.g., Klein et al., 2017; Myers et al., 2021; Myers & Norris, 2013, 2015; Qu et al., 2015; Scott et al., 2020; Stevens & Brenguier, 2009).

The method assumes that cloud-radiative anomalies at grid point r, $R(r)$, can be approximated as a linear function of anomalies in a set of M relevant cloud-controlling factors $\boldsymbol{X}_i$. Under this assumption, the cloud-radiative response per unit change in global surface air temperature T (i.e., the cloud feedback) can be written as

$$\frac{\mathrm{d}R(r)}{\mathrm{d}T} \approx \sum_{i=1}^{M} \frac{\partial R(r)}{\partial \boldsymbol{X}_i(r)} \cdot \frac{\mathrm{d}\boldsymbol{X}_i(r)}{\mathrm{d}T} = \sum_{i=1}^{M} \boldsymbol{\Theta}_i(r) \cdot \frac{\mathrm{d}\boldsymbol{X}_i(r)}{\mathrm{d}T}, \tag{1}$$

where $\boldsymbol{\Theta}_i$ represents the cloud-radiative *sensitivities* of R to the controlling factors—also referred to as *meteorological cloud-radiative kernels* by Scott et al. (2020) and Myers et al. (2021). Although we must rely on climate models to assess the controlling factor responses to warming, $\mathrm{d}\boldsymbol{X}_i/\mathrm{d}T$, we can estimate the cloud-radiative sensitivities $\boldsymbol{\Theta}_i$ observationally.

Following previous low-cloud literature (Klein et al., 2017, and references therein), we include the following six controlling factors: surface temperature, T_{sfc} (equivalent to sea-surface temperature over ocean grid points); estimated inversion strength, EIS; relative humidity at 700 hPa, RH_{700}; vertical pressure velocity at 700 hPa, ω_{700}; advection of the sea-surface temperature gradient by the near-surface wind, SSTadv; and near-surface wind speed, WS. EIS is computed from surface and 700 hPa temperature as well as sea-level pressure, following Wood and Bretherton (2006). The near-surface wind quantities are based on 10-m wind output from ERA5 and climate models.

We include all grid points between 60°S and 60°N in our analysis, thus minimizing issues with missing data and retrieval biases owing to high solar zenith angle. Furthermore, we exclude any data points where the monthly mean solar zenith angle exceeds 80°, calculated based on a local time of 10:30 a.m., the equator-crossing time of the Terra satellite (Loeb et al., 2018). For consistency, we apply this masking to all observations and climate model output. Note however that in contrast to previous cloud-controlling factor analyses of low-cloud feedback,

we include grid points from both land and ocean in our analysis. Over land, following Ceppi and Nowack (2021) instead of EIS we use the simpler metric of lower-tropospheric stability (LTS) as defined by Klein and Hartmann (1993), as the EIS metric involves assumptions that would only hold over the ocean surface. Furthermore, over land we also exclude SSTadv and WS as controlling factors, since surface turbulent moisture flux often scales with near-surface temperature advection and wind speed over the ocean, but not necessarily over land.

As another key difference from previous analyses, here instead of traditional multiple least-squares regression we use ridge regression (Hoerl & Kennard, 1970) with cross-validation to estimate the sensitivities $\boldsymbol{\Theta}_i$, where monthly cloud-induced radiative anomalies are regressed onto coincident controlling factor anomalies (see Text S3 in Supporting Information S1 for details). Importantly, ridge regression allows us to incorporate a relatively large number of predictors, while at the same time minimizing overfitting. Thus we include predictors not only from the target grid point r itself (as in previous studies), but also from a regional domain centered on point r. This has the benefit that we incorporate non-local influences on low clouds, particularly the known effect of upstream conditions (Lewis et al., 2023).

We use a 5×5 domain in grid point units (or $25° \times 25°$ in degree units)—see Text S3 in Supporting Information S1 for a discussion of this choice. Correspondingly, the predictors $\boldsymbol{X}_i(r)$ and the sensitivities $\boldsymbol{\Theta}_i(r)$ in Equation 1 are spatial vectors (i.e., regional maps), represented by bold symbols. As an example, regional sensitivity maps calculated for grid points in the Southern Hemispheric stratocumulus regimes are shown in Figure S3 in Supporting Information S1, showing a substantial influence of upstream T_{sfc} and EIS anomalies, in addition to the local effect. The definition and geographical distribution of the low-cloud regimes are detailed in Text S4 and Figure S4 in Supporting Information S1, respectively.

2.4. Climate Feedbacks and Sensitivity

In addition to the historical experiment, we also analyse abrupt-4xCO2 simulations to calculate low-cloud feedbacks as well as controlling factor responses per unit global warming (cf. Equation 1). For low-cloud feedbacks, we first calculate the abrupt-4xCO2 monthly longwave and shortwave low-cloud radiative anomalies (including their decomposition into amount and optical depth components; see Text S2 in Supporting Information S1) by convolving the ISCCP simulator data with the cloud-radiative kernels of Zelinka et al. (2012). We then aggregate these low-cloud radiative anomalies into annual means, and regress these values at each location onto annual-mean, global-mean temperature to assess the feedback (Gregory et al., 2004). We proceed similarly for the controlling factor responses. We use the full 150 years of the experiment, except for the IPSL-CM5A-MR model where only 140 years are available.

3. Evaluating the Cloud-Controlling Factor Analysis Framework

We test the predictive ability of our analysis framework in two ways: (a) using observations, by predicting out-of-sample extreme events in the observational record, similar to the approach followed by Myers et al. (2021) and Wall et al. (2022); (b) using climate models, by comparing predicted low-cloud feedback values against "actual" values diagnosed from abrupt-4xCO2 simulations.

Figure 2 shows an example of the first approach. We focus on the tropical marine trade cumulus regime as it covers a large fraction of the tropics, and its feedback is particularly uncertain (Myers et al., 2021; Vogel et al., 2022). To assess out-of-sample predictive skill, we rotate the training data set to exclude 1 year at a time, while training and cross-validating the ridge regressions over the remaining 19 years; we then use the resulting sensitivities to predict the low-cloud radiative anomalies R_{lowcld} for the excluded year, as per Equation 1. The statistical model does an excellent job predicting interannual R_{lowcld} variability out-of-sample over the marine trade cumulus regime (Figure 2b). We highlight the El-Niño period from July 2015 to June 2016, which is the warmest 12-month period in the MODIS record for the trade cumulus regime (Figure 2a). The corresponding R_{lowcld} anomalies are very well predicted, despite lying outside the range of values observed in other years (Figure 2b, red cross). The radiative anomalies are mainly associated with changes in T_{sfc}, with a secondary contribution from changes in SSTadv (Figure 2c).

Considering that future low-cloud feedback should be dominated by the contribution of surface warming (e.g., Myers et al., 2021), the result in Figure 2 lends confidence in the ability of the framework to accurately assess the sensitivity of low clouds to global warming. We obtain a qualitatively similar result in a separate out-of-sample

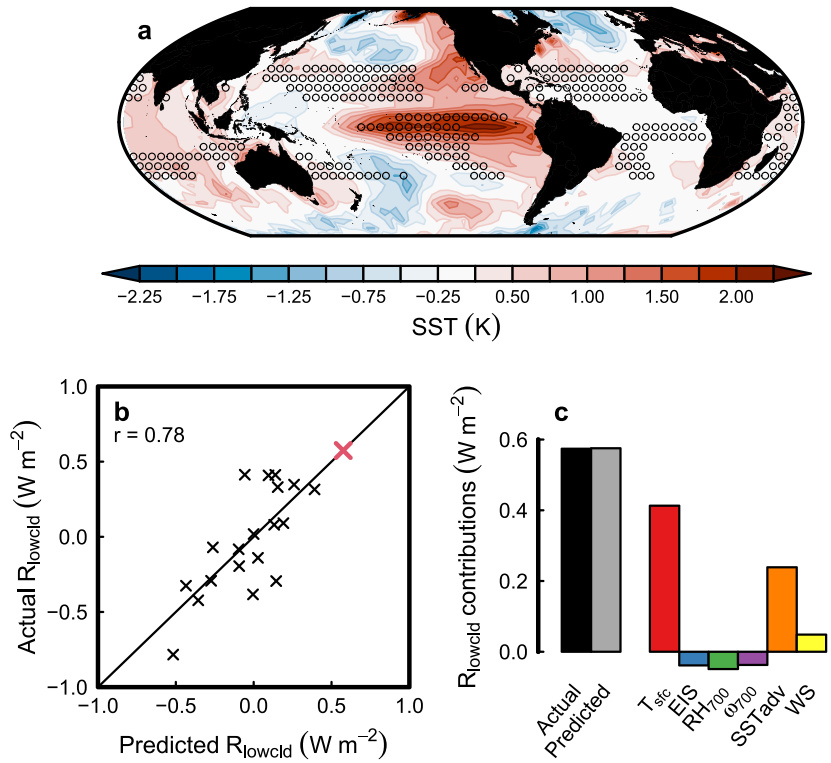

Figure 2. Out-of-sample prediction test of the observational trade cumulus sensitivities. (a) Map of annual-mean sea-surface temperature (SST) anomalies in the El-Niño year July 2015–June 2016 (shading), with tropical trade cumulus gridpoints denoted by circles. (b) Actual versus predicted MODIS net low-cloud radiative anomalies, R_{lowcld}, area-averaged over the trade cumulus domain and annually averaged between July 2002 and June 2022, with the July 2015–June 2016 period highlighted in red. Each data point was predicted out-of-sample by excluding the corresponding 12-month period from the training data set, and re-calculating the cloud-radiative sensitivities using the remaining 19 years of training data (cf. Section 2.3). (c) Contributions to the predicted R_{lowcld} anomalies in 2015–2016 from each of the six controlling factors. See Figure S5 in Supporting Information S1 for a similar out-of-sample prediction test for the stratocumulus regime.

prediction test for the stratocumulus regime, where we use the period July 2016–June 2017 as the warmest year in the record for that regime (Figure S5 in Supporting Information S1). Note that the sensitivities obtained by excluding either (or both) extreme years from the training sample are near-identical to those based on the full 20-year data set (not shown).

Now turning to climate models and considering the near-global domain 60°S–60°N, the ridge regression model performs well at predicting low-cloud feedback on a model-by-model basis (Figure 3a; Equation 1). Although the global-mean feedback is dominated by marine low clouds, the approach performs well over both ocean and land regions (Figure S6a in Supporting Information S1), and similarly for the amount and optical depth components of low-cloud feedback (Figure S7a in Supporting Information S1). Furthermore, both the geographical pattern and magnitude of cloud feedback are very well predicted for the CMIP mean (Figures S8a and S8d in Supporting Information S1), with an area-weighted spatial correlation coefficient of 0.85 between CMIP mean actual and predicted feedback.

4. Constraints on Low-Cloud Feedback

To constrain the wide range of low-cloud feedback values simulated by CMIP models, we use the sensitivities inferred from observations, combined with the controlling factor changes projected by climate models (Equation 1), and estimate uncertainty ranges following the method outlined in Text S5 in Supporting Information S1. Briefly, the uncertainty estimates account for both observational uncertainty (i.e., differences among satellite data sets) and methodological uncertainty (the scatter around the best-fit line in Figure 3a). As an illustration, the uncertainty in the global low-cloud feedback constraint is represented by the blue probability distribution curve along the *y*-axis of Figure 3a.

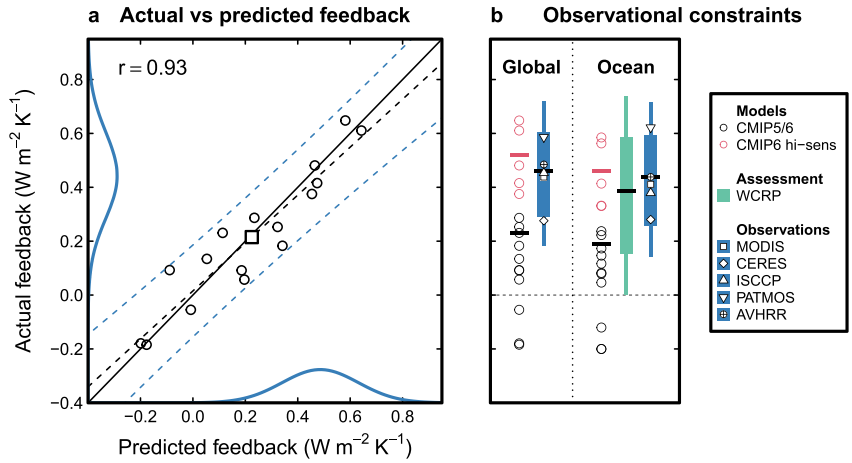

Figure 3. (a) Actual versus predicted global-mean net low-cloud feedback for 16 CMIP models (circles) and the multi-model mean (square). The values are for 60°S–60°N and scaled to global-mean values (Methods). The one-to-one line is shown in solid black. Dashed lines represent the least-squares fit (black) and the 5%–95% prediction interval (blue). Blue curves represent probability distributions for the observational estimates (amplitudes scaled arbitrarily). (b) Observational low-cloud feedback constraints (blue bars) for all low clouds (left), and marine low clouds only (right), compared to the CMIP model range (circles) and the WCRP constraint on marine low-cloud feedback from Sherwood et al. (2020) (green bar). Note that Sherwood et al. (2020) did not provide values for the land component of low-cloud feedback, and hence no WCRP constraint is available globally. Red circles denote high-sensitivity CMIP6 models. For the observational and WCRP constraints, thin and thick bars denote 90% and 66% confidence intervals, respectively, while horizontal bars denote medians. For CMIP models, horizontal bars denote multi-model means across all models (black) or across high-sensitivity models only (red).

We obtain a best estimate of global low-cloud feedback (land and ocean) of 0.45 W m^{-2} K^{-1} (Figure 3b; 90% range 0.18–0.72 W m^{-2} K^{-1}), about twice the CMIP mean value of 0.22 W m^{-2} K^{-1}. This difference is due to both cloud amount and optical depth feedbacks (Figures S7 and S8 in Supporting Information S1). For comparison with prior work, we also report ocean-only values; here the observational constraint is 0.42 (0.14–0.72) W m^{-2} K^{-1}, versus 0.18 W m^{-2} K^{-1} in the CMIP mean (note that unless otherwise noted, all feedback values reported here are scaled to global-mean contributions, rather than representing in-regime averages). Very similar constraints are obtained if the CMIP analysis is based on the AMIP experiment with observed SSTs instead of historical (Figure S9 in Supporting Information S1), suggesting the choice of SST boundary condition is not critical.

Our ocean-only estimate is considerably higher than the value reported by Myers et al. (2021) of 0.19 ± 0.12 W m^{-2} K^{-1}. Test calculations with a range of predictor domain sizes show that, as the predictor domain size grows, the central estimate for low-cloud feedback increases from a value similar to the Myers et al. (2021) estimate to around 0.45 W m^{-2} K^{-1} for domain sizes of 5 × 5 grid boxes and larger, with predictive skill increasing in parallel (see Figure S10 and Text S6 in Supporting Information S1). This domain size dependence is explained by changing low-cloud sensitivities to controlling factors, particularly surface temperature, and not by the inclusion of regional predictors (Figures S10–S13 and Text S6 in Supporting Information S1). Importantly, however, training the regression model with regional predictors allows for a more accurate estimation of the sensitivities, resulting in improved out-of-sample predictive skill, compared to a purely local regression model as in previous literature (Text S6 in Supporting Information S1).

Despite the discrepancy from previous observational work, our marine low-cloud feedback constraint is close to the central estimate published in the Sherwood et al. (2020) assessment (0.37 W m^{-2} K^{-1}). Hence, our results are consistent with the ECS estimate of Sherwood et al. (2020)—despite being at the high end of the CMIP distribution (Figure S14 in Supporting Information S1). Further discussion of the implications for ECS is provided in Text S7 in Supporting Information S1.

Compared with the previous generation of global climate models, CMIP6 features a set of models with particularly high ECS, mainly due to a comparatively strongly positive low-cloud feedback (Zelinka et al., 2020). Given that our observational constraint lies at the upper end of the distribution of CMIP values, we define a set of "high-

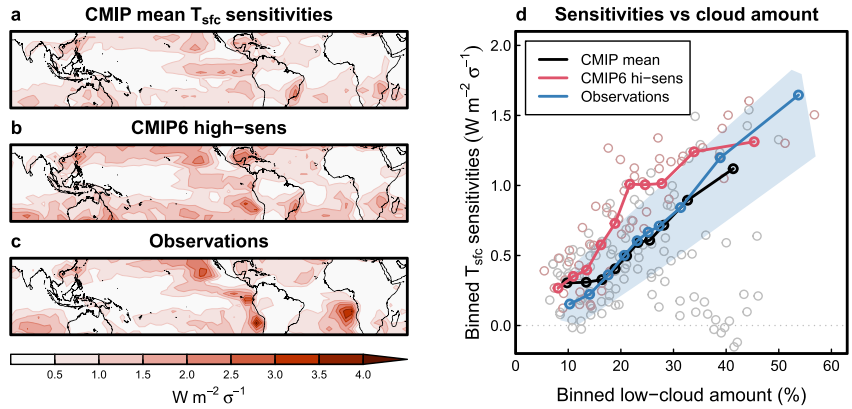

Figure 4. (a–c) Maps of net low-cloud radiative sensitivities to T_{sfc} over the tropics for (a) the CMIP mean, (b) CMIP high-sensitivity models, and (c) the mean observational estimates. The sensitivities are scaled by a one-standard-deviation anomaly (σ) in T_{sfc}, calculated from ERA5 reanalysis data during July 2002–June 2022. To produce global maps, we sum the sensitivities across each regional map (cf. Figure S3 in Supporting Information S1) to obtain one value per grid point. (d) Tropical (30°S–30°N) low-cloud T_{sfc} sensitivities binned by climatological low-cloud amount, using 10-percentile bins, over ocean grid points only. Black plotting symbols denote the CMIP multi-model mean, red the mean of the CMIP6 high-sensitivity models, and blue the mean observational coefficients. Model means are calculated after binning the data. Gray and light red circles indicate binned values from individual CMIP models, while the blue shading envelope represents the range from individual observational products. In all panels, for the low-cloud amount calculation in both CMIP models and observations, we exclude the lowest optical depth bin prior to integrating over all low-cloud histogram bins, to exclude known artifacts and biases in observational products (Pincus et al., 2012).

sensitivity" models, whose global-mean low-cloud feedback is in excess of 0.35 W m^{-2} K^{-1}. This set includes five models, all of which belong to CMIP6 (Table S2 in Supporting Information S1). Our selection criterion is admittedly arbitrary, and solely guided by the fact that on average, these models simulate a low-cloud feedback close to the observationally inferred value (Figure 3b, red symbols). Although our definition of "high-sensitivity" is based on low-cloud feedback rather than ECS, on average the five high-sensitivity models simulate much higher ECS values than the remaining 11 models (5.0 vs. 3.5 K).

On average, the high-sensitivity CMIP6 models are in good agreement with observations not just in terms of the near-global feedback, but also on a regime basis (Figure S15 in Supporting Information S1). The regime decomposition also reveals that the feedback differences between observations, high-sensitivity models and the CMIP mean cannot be ascribed to a single regime; the largest contribution comes from the midlatitudes, but tropical clouds also contribute substantially. It is also worth noting that in contrast to other recent observational studies that found evidence of weak-to-neutral trade cumulus feedback (Cesana & Del Genio, 2021; Myers et al., 2021; Vial et al., 2023; Vogel et al., 2022), our analysis points to a moderate positive feedback in this regime (Figure S15 in Supporting Information S1).

Differences in feedback between models and observations can be interpreted in terms of sensitivity differences to the controlling factors. In particular, the T_{sfc} sensitivities make a dominant contribution to the feedback (Figure S16 in Supporting Information S1). Considering maps of the cloud-radiative sensitivities, overall we find a strong qualitative resemblance between models and observations (Figure S17 in Supporting Information S1), and note that the sign and geographic distribution of these sensitivities are in broad agreement with previous work (Myers et al., 2021; Scott et al., 2020). Quantitatively, however, models tend to underestimate the magnitude of the sensitivities to T_{sfc}, EIS and SSTadv, particularly in stratocumulus regions (Figures 4a–4c and Figure S17 in Supporting Information S1), in agreement with Myers et al. (2021). Although CMIP6 high-sensitivity models generally have stronger T_{sfc} sensitivities than the average CMIP model, they also miss the particularly high sensitivities in stratocumulus regions (Figures 4a–4c and Figure S17 in Supporting Information S1). As shown in Figure S18 in Supporting Information S1, this underestimate comes from both the cloud amount and optical depth components of the T_{sfc} sensitivities, with a qualitatively similar result across observational data sets.

5. Relationship to Model Mean-State Bias

Previous work has pointed to present-day low-cloud biases, particularly in the amounts of trade cumulus and stratocumulus, as a driver of model error in low-cloud feedback (Cesana et al., 2019, 2023). Consistent with this idea, here we propose that the low-cloud feedback differences between CMIP models and observations are ultimately related to climatological differences in low-cloud amount. In Figure 4d, we plot the T_{sfc} sensitivities (over ocean gridpoints only, hence equivalent to SST) relative to the climatological low-cloud amount. For clarity, the values have been binned according to the percentiles of the low-cloud amount distribution. In both models and observations, there is a clear proportionality between low-cloud amount and T_{sfc} sensitivity: the more low cloud in the mean state, the stronger the sensitivity to T_{sfc}.

A possible reason for this is that, as mean-state low-cloud amount decreases, there is simply less low cloud to dissipate in response to increased T_{sfc}, resulting in a more weakly positive cloud-radiative sensitivity to T_{sfc}. Similar arguments have been made to explain the weakening of surface albedo feedback with warming in terms of decreasing snow and ice cover (Bloch-Johnson et al., 2015; Colman & McAvaney, 2009). An alternative (though not necessarily inconsistent) perspective on our finding is the mechanism of Brient and Bony (2012), where a decrease in cloud-top radiative cooling amplifies the low-cloud reduction with warming preferentially in regions with higher low-cloud amount, such as subtropical stratocumulus areas.

On average, CMIP models follow a very similar relationship compared to observations (blue and black curves in Figure 4d), even though the multi-model mean masks considerable inter-model differences (open gray circles). A key difference between models and observations, however, is that the observed relationship extends to much higher values of low-cloud amount and T_{sfc} sensitivity. The reason for this is evident from Figure 1: CMIP models substantially underestimate low-cloud amount in stratocumulus regions. It is worth noting that the CMIP low-cloud amount values in Figures 1 and 4d are based on satellite simulators, ensuring a fair comparison with observations. Note, however, that the relationship between mean-state low-cloud amount and low-cloud feedback does not hold across CMIP models (not shown): inter-model spread in low-cloud feedback is dominated not by the effect of mean-state cloudiness, but rather by model differences in cloud physics. This is in fact reflected in the different low-cloud sensitivities between the CMIP mean and the CMIP high-sensitivity mean, despite very similar mean-state cloud amounts (black and red curves in Figure 4d).

Figure 4d also reveals that the CMIP6 high-sensitivity models simulate the right global-mean feedback for the wrong reasons: rather than capturing the observed range of low-cloud amount, including the high values in tropical subsidence regions, they instead underestimate low-cloud amount like the typical CMIP model, while at the same time exhibiting unrealistically strong T_{sfc} sensitivities for a given low-cloud regime. This is qualitatively consistent with the recent observational findings of Vial et al. (2023) and Vogel et al. (2022) that high-sensitivity models exaggerate the marine low-cloud response to warming in moderate subsidence regimes, suggesting that their results are not necessarily at odds with our moderately positive trade cumulus feedback.

6. Summary and Conclusions

We perform a cloud-controlling factor analysis of low cloud-induced radiative anomalies to observationally constrain low-cloud feedback. The analysis indicates a moderately positive low-cloud feedback (central estimate of 0.45 W m^{-2} K^{-1}), substantially stronger than the CMIP mean (0.22 W m^{-2} K^{-1}). We find novel evidence that this model underestimate is linked to an underestimate of climatological low-cloud amount. On average, models and observations follow a common positive relationship between low-cloud amount and cloud-radiative sensitivity to sea-surface temperature (SST) across tropical regions; however, CMIP models fail to simulate the magnitudes of cloud amount and SST sensitivity observed in subsidence regions. Higher-sensitivity models compensate for a low-cloud amount deficit by simulating higher-than-average SST sensitivities for a given climatological low-cloud amount.

Different from previous work, the use of ridge regression allows us to include controlling factors from a regional domain around each target grid point. Since our data and methods are otherwise very similar to those of other recent cloud-controlling factor studies (e.g., Myers et al., 2021; Scott et al., 2020), it is the use of regional predictors that accounts for the stronger positive low-cloud feedback found here relative to prior studies. Given the dependence of the results on the choice of methodology, we suggest future work should test the robustness of our

findings using different analysis approaches. Nevertheless, the high out-of-sample predictive skill of our method in both models and observations lends confidence to our findings.

Data Availability Statement

All data sets used here are freely available online. Satellite cloud products were obtained from NASA (2022) (MODIS), NASA/LARC/SD/ASDC (2020) (CERES), Rossow et al. (2017) (ISCCP), Heidinger et al. (2014) (PATMOS-x), Stengel et al. (2019) (AVHRR-PM). ERA5 reanalysis data were obtained from Hersbach et al. (2023a, 2023b). Cloud-radiative kernels were downloaded from Zelinka (2021). Data from CMIP5 (Taylor et al., 2012) and CMIP6 (Eyring et al., 2016) were downloaded from https://esgf-node.llnl.gov. Equilibrium climate sensitivity (ECS) values are available from Zelinka (2022).

Acknowledgments
We are grateful to Greg Cesana, Ed Gryspeerdt and Joel Norris for helpful discussion of the results, and thank two anonymous reviewers for their constructive comments. We acknowledge support by the UK Government's Horizon Europe Funding Guarantee, Grant EP/Y036123/1 (PC), and the UK Natural Environmental Research Council Grants NE/V012045/1 (PC and PN) and NE/T006250/1 (PC). CJW received funding from the European Union's Horizon 2020 research and innovation programme under the Marie Skłodowska-Curie Grant 101019911. The work of MDZ was performed under the auspices of the U.S. Department of Energy by Lawrence Livermore National Laboratory under contract DE-AC52-07NA27344. This work used JASMIN, the UK collaborative data analysis facility. We acknowledge the World Climate Research Programme's Working Group on Coupled Modeling, which is responsible for CMIP, and we thank the climate modeling groups for producing and making available their model output. We also thank the Earth System Grid Federation (ESGF) for archiving the model output and providing access, and we thank the multiple funding agencies who support CMIP and ESGF.

References

Andersen, H., Cermak, J., Douglas, A., Myers, T. A., Nowack, P., Stier, P., et al. (2023). Sensitivities of cloud radiative effects to large-scale meteorology and aerosols from global observations. *Atmospheric Chemistry and Physics*, *23*(18), 10775–10794. https://doi.org/10.5194/acp-23-10775-2023

Bloch-Johnson, J., Pierrehumbert, R. T., & Abbot, D. S. (2015). Feedback temperature dependence determines the risk of high warming. *Geophysical Research Letters*, *42*(12), 4973–4980. https://doi.org/10.1002/2015GL064240

Bodas-Salcedo, A., Webb, M. J., Bony, S., Chepfer, H., Dufresne, J.-L., Klein, S. A., et al. (2011). COSP: Satellite simulation software for model assessment. *Bulletin of the American Meteorological Society*, *92*(8), 1023–1043. https://doi.org/10.1175/2011BAMS2856.1

Bony, S., & Dufresne, J.-L. (2005). Marine boundary layer clouds at the heart of tropical cloud feedback uncertainties in climate models. *Geophysical Research Letters*, *32*(20), L20806. https://doi.org/10.1029/2005GL023851

Boucher, O., Randall, D., Artaxo, P., Bretherton, C., Feingold, G., Forster, P., et al. (2013). Clouds and aerosols. In T. F. Stocker, D. Qin, G.-K. Plattner, M. Tignor, S. K. Allen, J. Boschung, et al. (Eds.), *Climate Change 2013: The Physical Science Basis. Contribution of Working Group I to the Fifth Assessment Report of the Intergovernmental Panel on Climate Change* (pp. 571–657). https://doi.org/10.1017/CBO9781107415324

Brient, F., & Bony, S. (2012). How may low-cloud radiative properties simulated in the current climate influence low-cloud feedbacks under global warming? *Geophysical Research Letters*, *39*(20). https://doi.org/10.1029/2012GL053265

Brient, F., & Schneider, T. (2016). Constraints on climate sensitivity from space-based measurements of low-cloud reflection. *Journal of Climate*, *29*(16), 5821–5835. https://doi.org/10.1175/JCLI-D-15-0897.1

Ceppi, P., & Nowack, P. (2021). Observational evidence that cloud feedback amplifies global warming. *Proceedings of the National Academy of Sciences of the United States of America*, *118*(30). https://doi.org/10.1073/pnas.2026290118

Cesana, G. V., Ackerman, A. S., Črnivec, N., Pincus, R., & Chepfer, H. (2023). An observation-based method to assess tropical stratocumulus and shallow cumulus clouds and feedbacks in CMIP6 and CMIP5 models. *Environmental Research Communications*, *5*(4), 045001. https://doi.org/10.1088/2515-7620/acc78a

Cesana, G. V., & Del Genio, A. D. (2021). Observational constraint on cloud feedbacks suggests moderate climate sensitivity. *Nature Climate Change*, *11*(3), 213–218. https://doi.org/10.1038/s41558-020-00970-y

Cesana, G. V., Del Genio, A. D., Ackerman, A. S., Kelley, M., Elsaesser, G., Fridlind, A. M., et al. (2019). Evaluating models' response of tropical low clouds to SST forcings using CALIPSO observations. *Atmospheric Chemistry and Physics*, *19*(5), 2813–2832. https://doi.org/10.5194/acp-19-2813-2019

Charney, J. G., Arakawa, A., Baker, D. J., Bolin, B., Dickinson, R. E., Goody, R. M., & Wunsch, C. I. (1979). Carbon dioxide and climate (Tech. Rep.). https://doi.org/10.17226/12181

Colman, R., & McAvaney, B. (2009). Climate feedbacks under a very broad range of forcing. *Geophysical Research Letters*, *36*(1). https://doi.org/10.1029/2008GL036268

Črnivec, N., Cesana, G. V., & Pincus, R. (2023). Evaluating the representation of tropical stratocumulus and shallow cumulus clouds as well as their radiative effects in CMIP6 models using satellite observations. *Journal of Geophysical Research: Atmospheres*, *128*(23), e2022JD038437. https://doi.org/10.1029/2022JD038437

Dormann, C. F., Elith, J., Bacher, S., Buchmann, C., Carl, G., Carré, G., et al. (2013). Collinearity: A review of methods to deal with it and a simulation study evaluating their performance. *Ecography*, *36*(1), 27–46. https://doi.org/10.1111/j.1600-0587.2012.07348.x

Eyring, V., Bony, S., Meehl, G. A., Senior, C. A., Stevens, B., Stouffer, R. J., & Taylor, K. E. (2016). Overview of the coupled model intercomparison project phase 6 (CMIP6) experimental design and organization. *Geoscientific Model Development*, *9*(5), 1937–1958. https://doi.org/10.5194/gmd-9-1937-2016

Garay, M. J., de Szoeke, S. P., & Moroney, C. M. (2008). Comparison of marine stratocumulus cloud top heights in the southeastern Pacific retrieved from satellites with coincident ship-based observations. *Journal of Geophysical Research*, *113*(D18). https://doi.org/10.1029/2008JD009975

Gregory, J. M., Ingram, W. J., Palmer, M. A., Jones, G. S., Stott, P. A., Thorpe, R. B., et al. (2004). A new method for diagnosing radiative forcing and climate sensitivity. *Geophysical Research Letters*, *31*(3), L03205. https://doi.org/10.1029/2003GL018747

Heidinger, A. K., Foster, M. J., Walther, A., Zhao, X., & NOAA CDR Program. (2014). NOAA climate data record (CDR) of cloud properties from AVHRR Pathfinder Atmospheres—DatasetExtended (PATMOS-x), version 5.3 [Dataset]. https://doi.org/10.7289/V5348HCK

Hersbach, H., Bell, B., Berrisford, P., Biavati, G., Horányi, A., Muñoz Sabater, J., et al. (2023a). ERA5 monthly averaged data on pressure levels from 1940 to present [Dataset]. https://doi.org/10.24381/cds.6860a573

Hersbach, H., Bell, B., Berrisford, P., Biavati, G., Horányi, A., Muñoz Sabater, J., et al. (2023b). ERA5 monthly averaged data on single levels from 1940 to present [Dataset]. https://doi.org/10.24381/cds.f17050d7

Hersbach, H., Bell, B., Berrisford, P., Hirahara, S., Horányi, A., Muñoz-Sabater, J., et al. (2020). The ERA5 global reanalysis. *Quarterly Journal of the Royal Meteorological Society*, *146*(730), 1999–2049. https://doi.org/10.1002/qj.3803

Hoerl, A. E., & Kennard, R. W. (1970). Ridge regression: Biased estimation for nonorthogonal problems. *Technometrics*, *12*(1), 55–67. https://doi.org/10.1080/00401706.1970.10488634

Klein, S. A., Hall, A., Norris, J. R., & Pincus, R. (2017). Low-cloud feedbacks from cloud-controlling factors: A review. *Surveys in Geophysics*, *38*(6), 1–23. https://doi.org/10.1007/s10712-017-9433-3

Klein, S. A., & Hartmann, D. L. (1993). The seasonal cycle of low stratiform clouds. *Journal of Climate*, *6*(8), 1587–1606. https://doi.org/10.1175/1520-0442(1993)006⟨1587:TSCOLS⟩2.0.CO;2

Klein, S. A., Zhang, Y., Zelinka, M. D., Pincus, R., Boyle, J., & Gleckler, P. J. (2013). Are climate model simulations of clouds improving? An evaluation using the ISCCP simulator. *Journal of Geophysical Research: Atmospheres*, *118*(3), 1329–1342. https://doi.org/10.1002/jgrd.50141

Konsta, D., Dufresne, J.-L., Chepfer, H., Vial, J., Koshiro, T., Kawai, H., et al. (2022). Low-level marine tropical clouds in six CMIP6 models are too few, too bright but also too compact and too homogeneous. *Geophysical Research Letters*, *49*(11), e2021GL097593. https://doi.org/10.1029/2021GL097593

Kuma, P., Bender, F. A.-M., Schuddeboom, A., McDonald, A. J., & Seland, Ø. (2023). Machine learning of cloud types in satellite observations and climate models. *Atmospheric Chemistry and Physics*, *23*(1), 523–549. https://doi.org/10.5194/acp-23-523-2023

Lewis, H., Bellon, G., & Dinh, T. (2023). Upstream large-scale control of subtropical low-cloud climatology. *Journal of Climate*, *36*(10), 3289–3303. https://doi.org/10.1175/JCLI-D-22-0676.1

Loeb, N. G., Doelling, D. R., Wang, H., Su, W., Nguyen, C., Corbett, J. G., et al. (2018). Clouds and the Earth's radiant energy system (CERES) energy balanced and filled (EBAF) top-of-atmosphere (TOA) edition-4.0 data product. *Journal of Climate*, *31*(2), 895–918. https://doi.org/10.1175/JCLI-D-17-0208.1

Myers, T. A., & Norris, J. R. (2013). Observational evidence that enhanced subsidence reduces subtropical marine boundary layer cloudiness. *Journal of Climate*, *26*(19), 7507–7524. https://doi.org/10.1175/JCLI-D-12-00736.1

Myers, T. A., & Norris, J. R. (2015). On the relationships between subtropical clouds and meteorology in observations and CMIP3 and CMIP5 models. *Journal of Climate*, *28*(8), 2945–2967. https://doi.org/10.1175/JCLI-D-14-00475.1

Myers, T. A., & Norris, J. R. (2016). Reducing the uncertainty in subtropical cloud feedback. *Geophysical Research Letters*, *43*(5), 2144–2148. https://doi.org/10.1002/2015GL067416

Myers, T. A., Scott, R. C., Zelinka, M. D., Klein, S. A., Norris, J. R., & Caldwell, P. M. (2021). Observational constraints on low cloud feedback reduce uncertainty of climate sensitivity. *Nature Climate Change*, *11*(6), 501–507. https://doi.org/10.1038/s41558-021-01039-0

Nam, C., Bony, S., Dufresne, J.-L., & Chepfer, H. (2012). The "too few, too bright" tropical low-cloud problem in CMIP5 models. *Geophysical Research Letters*, *39*(21). https://doi.org/10.1029/2012GL053421

NASA. (2022). MODIS (Aqua/Terra) cloud properties level 3 monthly, 1 × 1 degree grid [Dataset]. https://doi.org/10.5067/MODIS/MCD06COSP_M3_MODIS.062

NASA/LARC/SD/ASDC. (2020). CERES monthly daytime mean regionally averaged Terra and Aqua TOA fluxes and associated cloud properties stratified by optical depth and effective pressure Edition4A [Dataset]. https://doi.org/10.5067/Terra-Aqua/CERES/FLUXBYCLDTYP-MONTH_L3.004A

Nowack, P., Ceppi, P., Davis, S. M., Chiodo, G., Ball, W., Diallo, M. A., et al. (2023). Response of stratospheric water vapour to warming constrained by satellite observations. *Nature Geoscience*, *16*(7), 577–583. https://doi.org/10.1038/s41561-023-01183-6

Pincus, R., Hubanks, P. A., Platnick, S., Meyer, K., Holz, R. E., Botambekov, D., & Wall, C. J. (2023). Updated observations of clouds by MODIS for global model assessment. *Earth System Science Data*, *15*(6), 2483–2497. https://doi.org/10.5194/essd-15-2483-2023

Pincus, R., Platnick, S., Ackerman, S. A., Hemler, R. S., & Patrick Hofmann, R. J. (2012). Reconciling simulated and observed views of clouds: MODIS, ISCCP, and the limits of instrument simulators. *Journal of Climate*, *25*(13), 4699–4720. https://doi.org/10.1175/JCLI-D-11-00267.1

Qu, X., Hall, A., Klein, S. A., & DeAngelis, A. M. (2015). Positive tropical marine low-cloud cover feedback inferred from cloud-controlling factors. *Geophysical Research Letters*, *42*(18), 7767–7775. https://doi.org/10.1002/2015GL065627

Rossow, W., Walker, A., Golea, V., Knapp, K., Young, A., Inamdar, A., et al. (2017). International satellite cloud climatology project climate data record, H-series [Dataset]. https://doi.org/10.7289/V5QZ281S

Scott, R. C., Myers, T. A., Norris, J. R., Zelinka, M. D., Klein, S. A., Sun, M., & Doelling, D. R. (2020). Observed sensitivity of low-cloud radiative effects to meteorological perturbations over the global oceans. *Journal of Climate*, *33*(18), 7717–7734. https://doi.org/10.1175/JCLI-D-19-1028.1

Sherwood, S., Webb, M. J., Annan, J. D., Armour, K. C., Forster, P. M., Hargreaves, J. C., et al. (2020). An assessment of Earth's climate sensitivity using multiple lines of evidence. *Reviews of Geophysics*, *58*(4), 1–92. https://doi.org/10.1029/2019RG000678

Siler, N., Po-Chedley, S., & Bretherton, C. S. (2018). Variability in modeled cloud feedback tied to differences in the climatological spatial pattern of clouds. *Climate Dynamics*, *50*(3–4), 1–12. https://doi.org/10.1007/s00382-017-3673-2

Stengel, M., Stapelberg, S., Sus, O., Finkensieper, S., Würzler, B., Philipp, D., et al. (2020). Cloud_cci advanced very high resolution radiometer post meridiem (AVHRR-PM) dataset version 3: 35-year climatology of global cloud and radiation properties. *Earth System Science Data*, *12*(1), 41–60. https://doi.org/10.5194/essd-12-41-2020

Stengel, M., Sus, O., Stapelberg, S., Finkensieper, S., Würzler, B., Philipp, D., et al. (2019). ESA cloud climate change initiative (ESA cloud_cci) data: Cloud_cci AVHRR-PM L3C/L3U CLD_PRODUCTS v3.0 [Dataset]. https://doi.org/10.5676/DWD/ESA_Cloud_cci/AVHRR-PM/V003

Stevens, B., & Brenguier, J.-L. (2009). Cloud controlling factors—Low clouds. In J. Heintzenberg & R. J. Charlson (Eds.), *Clouds in the perturbed climate system: Their relationship to energy balance, atmospheric dynamics, and precipitation* (pp. 173–196). MIT Press.

Sun, M., Doelling, D. R., Loeb, N. G., Scott, R. C., Wilkins, J., Nguyen, L. T., & Mlynczak, P. (2022). Clouds and the Earth's radiant energy system (CERES) FluxByCldTyp Edition 4 data product. *Journal of Atmospheric and Oceanic Technology*, *39*(3), 303–318. https://doi.org/10.1175/JTECH-D-21-0029.1

Taylor, K. E., Stouffer, R. J., & Meehl, G. A. (2012). An overview of CMIP5 and the experiment design. *Bulletin of the American Meteorological Society*, *93*(4), 485–498. https://doi.org/10.1175/BAMS-D-11-00094.1

Vial, J., Albright, A. L., Vogel, R., Musat, I., & Bony, S. (2023). Cloud transition across the daily cycle illuminates model responses of trade cumuli to warming. *Proceedings of the National Academy of Sciences of the United States of America*, *120*(8), e2209805120. https://doi.org/10.1073/pnas.2209805120

Vogel, R., Albright, A. L., Vial, J., George, G., Stevens, B., & Bony, S. (2022). Strong cloud–circulation coupling explains weak trade cumulus feedback. *Nature*, *612*(7941), 696–700. https://doi.org/10.1038/s41586-022-05364-y

Wall, C. J., Norris, J. R., Possner, A., McCoy, D. T., McCoy, I. L., & Lutsko, N. J. (2022). Assessing effective radiative forcing from aerosol–cloud interactions over the global ocean. *Proceedings of the National Academy of Sciences of the United States of America*, *119*(46), e2210481119. https://doi.org/10.1073/pnas.2210481119

Wilson Kemsley, S., Ceppi, P., Andersen, H., Cermak, J., Stier, P., & Nowack, P. (2024). A systematic evaluation of high-cloud controlling factors. *Atmospheric Chemistry and Physics*, *24*(14), 8295–8316. https://doi.org/10.5194/acp-24-8295-2024

Wood, R., & Bretherton, C. S. (2006). On the relationship between stratiform low cloud cover and lower-tropospheric stability. *Journal of Climate*, *19*(24), 6425–6432. https://doi.org/10.1175/JCLI3988.1

Young, A. H., Knapp, K. R., Inamdar, A., Hankins, W., & Rossow, W. B. (2018). The international satellite cloud climatology project H-series climate data record product. *Earth System Science Data*, *10*(1), 583–593. https://doi.org/10.5194/essd-10-583-2018

Zelinka, M. D. (2021). Mzelinka/cloud-radiative-kernels: Sep 17, 2021 release [Dataset]. https://doi.org/10.5281/zenodo.5514137

Zelinka, M. D. (2022). Mzelinka/cmip56_forcing_feedback_ecs: Jun 15, 2022 release [Dataset]. https://doi.org/10.5281/zenodo.6647291

Zelinka, M. D., Klein, S. A., & Hartmann, D. L. (2012). Computing and partitioning cloud feedbacks using cloud property histograms. Part I: Cloud radiative kernels. *Journal of Climate*, *25*(11), 3715–3735. https://doi.org/10.1175/JCLI-D-11-00248.1

Zelinka, M. D., Myers, T. A., McCoy, D. T., Po-Chedley, S., Caldwell, P. M., Ceppi, P., et al. (2020). Causes of higher climate sensitivity in CMIP6 models. *Geophysical Research Letters*, *47*(1). https://doi.org/10.1029/2019GL085782

Zhang, M. H., Lin, W. Y., Klein, S. A., Bacmeister, J. T., Bony, S., Cederwall, R. T., et al. (2005). Comparing clouds and their seasonal variations in 10 atmospheric general circulation models with satellite measurements. *Journal of Geophysical Research*, *110*(D15). https://doi.org/10.1029/2004JD005021

References From the Supporting Information

Bishop, C. M. (2006). *Pattern recognition and machine learning*. Springer.

Zelinka, M. D., Zhou, C., & Klein, S. A. (2016). Insights from a refined decomposition of cloud feedbacks. *Geophysical Research Letters*, *43*(17), 9259–9269. https://doi.org/10.1002/2016GL069917